Design Considerations of Sub-mW Indoor Light Energy Harvesting for Wireless Sensor Systems

W. S. WANG, T. O'DONNELL, N. WANG, and M. HAYES
Tyndall National Institute
and
B. O'FLYNN and C. O'MATHUNA
Clarity Center for Sensor Web Technologies

6

For most wireless sensor networks, one common and major bottleneck is the limited battery lifetime. The frequent maintenance efforts associated with battery replacement significantly increase the system operational and logistics cost. Unnoticed power failures on nodes will degrade the system reliability and may lead to system failure. In building management applications, to solve this problem, small energy sources such as indoor light energy are promising to provide long-term power to these distributed wireless sensor nodes. This article provides comprehensive design considerations for an indoor light energy harvesting system for building management applications. Photovoltaic cells characteristics, energy storage units, power management circuit design, and power consumption pattern of the target mote are presented. Maximum power point tracking circuits are proposed which significantly increase the power obtained from the solar cells. The novel fast charge circuit reduces the charging time. A prototype was then successfully built and tested in various indoor light conditions to discover the practical issues of the design. The evaluation results show that the proposed prototype increases the power harvested from the PV cells by 30% and also accelerates the charging rate by 34% in a typical indoor lighting condition. By entirely eliminating the rechargeable battery as energy storage, the proposed system would expect an operational lifetime 10–20 years instead of the current less than 6 months battery lifetime.

Categories and Subject Descriptors: C.2.3 [**Computer-Communication Networks**]: Network Operation—*Network management*; C.2.1 [**Computer-Communication Networks**]: Network Architecture and Design—*Wireless communication*; C.3 [**Computer Systems Organization**]: Special-Purpose and Application-Based Systems—*Real-time and embedded systems*; C.4 [**Computer Systems Organization**]: Performance of Systems—*Design studies*

General Terms: Design, Experimentation, Measurement, Performance

This work has been funded by Scientific Foundation Ireland through a research project ITOBO (398-CRP) and Enterprise Ireland research project BuildWise (RI2407).
Authors' addresses: W. S. Wang (corresponding author), T. O'Donnell, N. Wang, and M. Hayes, Tyndall National Institute, Cork, Ireland; email: wensi.wang@tyndall.ie; B. O'Flynn and C. O'Mathuna, Clarity Center for Sensor Web Technologies, Cork, Ireland.

DOI 10.1145/1773814.1773817 http://doi.acm.org/10.1145/1773814.1773817

Additional Key Words and Phrases: Design consideration, energy harvesting, PV cells wireless sensor node, maximum power point tracking, indoor light illuminance, supercapacitor

ACM Reference Format:
Wang, W. S., O'Donnell, T., Wang, N., Hayes, M., O'Flynn, B., and O'Mathuna, C. 2010. Design considerations of sub-mW indoor light energy harvesting for wireless sensor systems. ACM J. Emerg. Technol. Comput. Syst. 6, 1, Article 6 (June 2010), 26 pages.
DOI = 10.1145/1773814.1773817 http://doi.acm.org/10.1145/1773814.1773817

1. INTRODUCTION

In the past few years, Wireless Sensor Networks (WSN) have emerged from the research domain to providing commercial solutions for many real-world applications. Currently, several WSN products have already been deployed in volume in commercial applications [Krikke 2005]. Among the anticipated applications, one of the areas of greatest potential is in Building Energy Management (BEM). By monitoring artificial lighting, temperature, carbon dioxide level, relative humidity, positioning of external shading devices, and resultant actuation, a considerable percentage of energy can be saved and human comfort levels can be improved. For example, about 35% of North America's energy usage [Energy Conservation Management, Inc. 2006] and over 37% of CO_2 emissions [King et al. 2007] are attributed to the running of residential and commercial buildings. It has been estimated that the usage of intelligent sensor networks can result in 15–20% savings in total energy usage [Grigg and Slater 2007]. Due to such potential financial benefits and the political "green agenda", intensive research interests have been focused on this area [Menzel et al. 2008].

The ease of deployment may enable these radio-frequency-based sensor systems to replace most of the current "wired" (cable-connected) sensor systems in the foreseeable future. However, one major bottleneck for all WSN deployments has yet to be solved. This problem is the limited system lifetime due to the insufficient energy capacity of the small form factor battery power supply. For example, a wireless sensor node designed at the Tyndall Institute with temperature and relative humidity sensors [Barton et al. 2005] consumes an average of 250 μW when it operates on a low 0.1% duty cycle (fraction of time when sensing and transmitting occurs). Theoretically, powering from two standard 2000 mAh AA battery cells requires battery replacement approximately every 200 days. In practice, however, the battery lifetime is even shorter due to leakage currents, temperature fluctuations, environmental humidity, and other variable factors [Doyle et al. 1993]. With the increasing deployment scale of nodes in WSN systems, the market demands a "deploy and forget" solution requiring the elimination of a battery replacement maintenance cycle. Energy harvesting technology could lead to this possibility of self-sustaining "infinite" lifetime motes, or at least the prolongation on the life span between battery replacements. This is becoming a significant focus area in WSN research in recent years because of the necessity of bridging the gap between the continuous power consumption of the mote and the limited available energy from the battery technology [Hayes et al 2009].

Table I. Power Density of Various Energy Harvesting Technologies

Energy Sources	Power Density
Indoor light (office 500lux) (Randall 2005)	$300\mu W/cm^2$
Outdoor light (Standard, AM1.5) (Myers et al. 2000)	$100mW/cm^2$
Shoe Insert Piezoelectric (Shenck and Paradiso 2001)	$300\mu W/cm^3$
Mechanical vibration (Pereyma 2007)	$45\mu W/cm^3$
Thermoelectric (10°C gradient) (Roundy 2004)	$15\mu W/cm^3$

Many types of ambient energy sources are available. However, light illuminance [Randall 2005], temperature gradients [Doms et al. 2009], and vibrations [Roundy et al. 2005], have drawn the most attention within the research community, as a result of their relatively high technology readiness levels. For example, Table I shows the power density which has been obtained from different energy harvesting sources potentially available in BEM applications, that is, indoor office illuminance, outdoor illuminance, human and machine vibration energy, building thermal energy.

Each of the energy sources and energy harvesting technologies has different advantages and drawbacks. Detailed comparisons of the energy density from the various sources have been presented [Rahimi et al. 2003]. Although indoor light energy has a relatively small power density, it is a significantly more mature technology. In addition, indoor light energy is the most common energy source which exists ubiquitously in most office and residential environments. The commercial availability of photovoltaic panels is also better than piezoelectric generators and thermoelectric generators. However, the majority of research in light energy harvesting is mainly focused on relatively large-scale outdoor applications [Raghunathan et al. 2006].

Unlike the outdoor application, for indoor conditions, the overall light energy density is inherently limited. For example, a typical light energy density in a fluorescent lighting condition (500 lux) is one to two orders of magnitude lower than the outdoor light energy density [Hermle et al. 2003]. This together with low light energy conversion efficiency in indoor environments makes indoor light energy harvesting very challenging. For indoor light energy harvesting applications, it is therefore important to optimize system design so an energy harvester can provide sufficient energy to the WSN in low illuminance levels. In addition, many other system design issues require considerations, such as small form factor, output voltage level, capacity of the energy storage, cost efficiency, and "plug and play" ability. Furthermore, these factors are not isolated, but are dynamically interrelated. However, compared to well-addressed outdoor macropower systems, few thorough studies have been carried out on these design issues and the trade-offs between them. Therefore, this article mainly addresses the design considerations of light energy powered wireless sensor mote devices in low illuminance indoor conditions for BEM applications.

In this article, firstly, the target wireless sensor system (the Tyndall 25 mm WSN) is introduced and the design requirements and system architecture of the proposed indoor light energy harvester discussed. Then the characteristics of typical indoor light energy sources are analyzed and the choice of the Photovoltaic (PV) panels based on these characteristics reviewed.

Maximization of the energy available through the use of Maximum Power Point Tracking (MPPT) is discussed and the energy gains achievable from several maximum power point tracking approaches are analyzed. The considerations for the choice of the energy storage component are also discussed and the trade-offs are highlighted. Based on these considerations, a design solution for an indoor light powered wireless sensor system is presented. Operational results of the energy harvesting devices are shown and the performance is evaluated.

2. RELATED WORK

Light energy powered WSN system design is an area of active research interest. Several light energy harvesting systems for WSN have been proposed and published recently.

"Helimote" presented by Raghunathan et al. [2005] is one of the first proposed light energy harvesting powered WSN systems. It features a simple outdoor solar panel powered mote system design, directly connecting the solar cell to the energy storage. Energy storage in Helimote is achieved using NiMH rechargeable batteries. It lacks an MPP tracking function, and can only charge the battery when the solar panel output voltage is 0.7 V higher than the battery voltage [Raghunathan et al. 2005].

"Prometheus" presented by Jiang et al. [2005] uses a design similar to Helimote, but it features a hybrid energy storage: combination of a Li-Polymer rechargeable battery and a 22 F supercapacitor. Certain control logic is used to charge the battery from the supercapacitor when the latter is fully charged versus directly feeding the battery to the load when supercapacitor voltage is lower than a defined threshold voltage. This method prolongs the battery lifetime. Similar to the Helimote, it also lacks an MPPT function and requires a high charging voltage [Jiang et al. 2005].

"Everlast" presented by Simjee and Chou [2008] implements a design eliminating the rechargeable battery. The energy storage element is a 100 F supercapacitor. The Everlast design employs an MPPT algorithm running on the mote's microcontroller. The MPPT is accurate and operates at a high speed. However, this MPPT method requires a much higher power level from the PV cells and is not a suitable choice for indoor light energy harvesting [Simjee and Chou 2008].

These three light energy harvesting systems discussed before are only suitable for operation in outdoor conditions. The system power consumption and output power of the PV cells are well above the 100 mW level.

A solar powered mote system called "Ambimax" proposed by Park and Chou [2006] uses multiple power sources including solar energy and wind energy. The power sources were managed by a common power conditioning unit. Ambimax automatically tracks the maximum power point without using the microcontroller of the WSN. The energy storage in this system is a supercapacitor and Li-Polymer battery combination [Park and Chou 2006]. Similar to Prometheus, the system lifetime of this design would also be limited by the battery lifetime. The MPPT subsystem requires a current consumption in the mA range, which

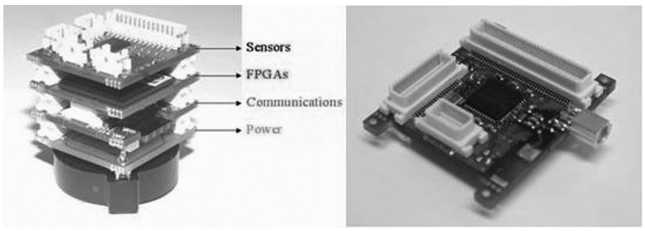

Fig. 1. Tyndall wireless sensor node.

is more than an order of magnitude higher than the power consumption of the proposed Tyndall motes (load).

Brunelli et al. [2009] presented a system similar to the design used in this article. A 50 F supercapacitor is used as the energy storage. The PWM controlled MPPT circuit implements the fractional open circuit voltage method. The carefully simulated and implemented MPPT subsystem only requires mW-level power consumption. However, due to the inherent relatively high power consumption of the PWM circuits, potential for further MPPT circuit power consumption reduction is limited [Brunelli et al. 2009].

3. TYNDALL WIRELESS SENSOR NETWORKS

The efficient design of any energy harvesting system can only be achieved through a thorough understanding of its load, the wireless sensor node in operation. In this section, the energy usage of the wireless sensor node and its usage pattern in various test configurations is presented. The analysis is based on the experimental results obtained from the Tyndall mote, as shown in Figure 1. The Tyndall mote has a multiple-layer design with extension/replacement ability and can be configured to take different power layers and sensor layers with only minor changes on hardware and software [Harte et al. 2007]. The Atmega128 series microcontroller and Zigbee transceiver CC2420 were used in the mote. For initial BEM application, a temperature and relatively humidity (RH) sensor (Sensirion SHT71) and a thermal resistor (AVX NB20R) were used on the sensor layer.

In general, the wireless sensor node is a microcontroller controlled sensing and communication module which is required to sense and transmit its readings periodically. It therefore typically has at least two different modes, consisting of: (i) an active mode where sensing and data transmission takes place and (ii) a low-power sleep mode which it adopts between sensing intervals. During its sensing and transmitting/receiving mode, the power consumption is much higher than in sleep mode. In the case of the Tyndall mote the active power consumption is 1700 times higher than its average sleep mode power consumption, as shown in Table II. As a result, most wireless sensor nodes adopt an asymmetric ratio duty cycling operation, with a much longer sleep mode time than active mode time. In the proposed BEM application, two types of measurements are required, namely, periodic parameter sampling and event response. Since the event response requires the mote to stay in active mode for most of the lifetime to dynamically respond to the nonperiodical event, the

Table II. Tyndall Mote Power Consumption for Building Electricity Usage Monitoring

	Voltage (V)	Power Consumption (mW)	Time (sec)	Energy Consumption (mJ)	Ratio Duty Cycle	Percentage of Energy Consumption
Active (Sensor, microcontroller & transceiver)	3.0	96.2	0.039	3.75	0.065%	53.6%
Sleep	3.0	0.0541	60	3.24	99.935%	46.4%
Average	3.0	0.116	60.039	6.99	100%	100%

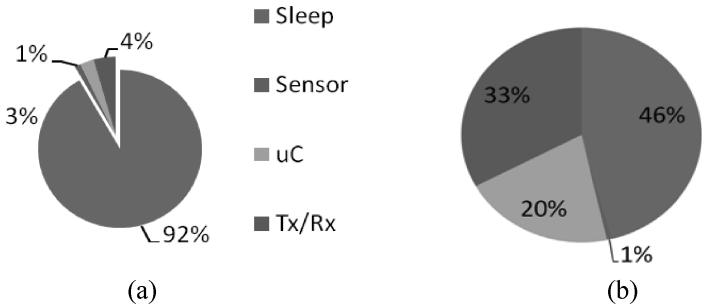

Fig. 2. Tyndall wireless sensor node power consumption pie chart: (a) 1 sample per 15 minutes, P = 65 μW; (b) 1 sample per 1 minute, P = 116 μW.

requirement of the parameter sampling rate is higher when compared to periodic parameter sampling applications. In this article, only the parameter sampling applications are discussed. For room temperature monitoring, the sampling rate is once every 15 minutes; the energy usage monitoring requires 1 sample every minute. Due to the structural similarity between the Tyndall mote and other commercial available motes like the Moteiv Tmote Sky (Temote sky, SNM website) and Crossbow MicaZ (MicaZ, SNM website), the power consumption is also comparable. The difference on the average power consumption between Tyndall mote, Tmote Sky, and MicaZ mote is within the 20% range.

The overall power consumption of the wireless sensor node therefore highly depends on the duty cycle, D, with the average power consumption approximated by

$$P_{average} = P_{active} \cdot D + P_{sleep} \cdot (1 - D), \tag{1}$$

where $P_{average}$ is the average power consumption of the mote, P_{active} is the sensing and transmission power consumption, and P_{sleep} is the sleep mode power consumption. D is the duty cycle defined as the ratio of the time required to sense and transmit a single sample to the sampling period. In the proposed BEM system, the different duty cycle requirements result in different power consumption. For 1 minute intervals, the average power consumption of the Tyndall mote is 116.3 μW, but for 15 minutes per measurement, the average power consumption is only 65.3 μW. It is worth noting that the sleep mode consumes a large portion of the total energy as shown in Figure 2, measuring 46% (1 minute intervals) and 92% (15 minutes intervals) of the total energy, respectively. Since the proposed deployment scenario requires the mote to

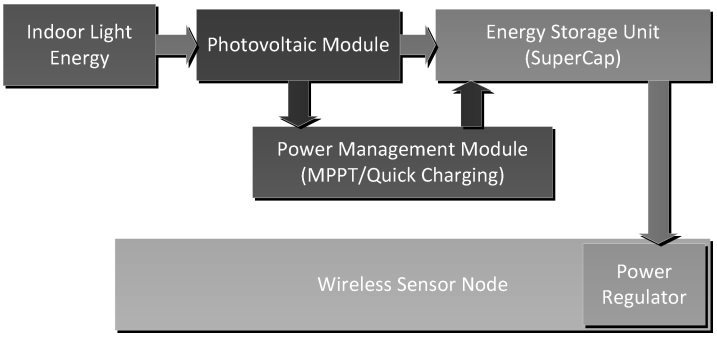

Fig. 3. System architechture.

operate over a long period of time, the mote was programmed to enter "deep sleep" mode after each transmission in order to save as much energy as possible. In this mode, the mote cannot respond to the external interrupt, therefore an external timer was used to activate the mote when required. The typical power consumption in this mode is 15 μW.

The average power consumption is highly sensitive to the operation duty cycle, and the sleep mode power consumption is critical for low duty cycle applications. These two features distinctly affect the design considerations and system architecture of the energy harvester system. The effects are introduced in later sections.

4. LIGHT POWERED WSN SYSTEM ARCHITECTURE

A typical light energy harvesting system will consist of several parts, as illustrated in Figure 3. These parts include a photovoltaic module, an energy storage unit, power management circuits, and the wireless sensor node as the load.

The operational environment of this light powered WSN prototype is a typical office environment. The most common light energy sources are the overhead fluorescent lights. To harvest the energy from the fluorescent lights, photovoltaic cells that are well matched to the fluorescent spectrum and that can deliver high efficiency at low illuminance levels are required.

The typical WSN may have several orders of magnitude difference between the peak power requirements during active mode and the average power requirement over the entire cycle. The PV cells should be sized in order to provide the average power, and therefore an additional energy storage element is required to provide the peak active power. The energy storage unit should also be capable of providing power to the system during darkness.

Photovoltaic cells have a similar behavior to a voltage controlled current source, thus having a relatively steady voltage output and a variable current output depending on the light illuminance. Due to this current source behavior, the output power of the PV cell is subject to the operational voltage on the PV cells. Without optimization, the voltage on the PV cells may not operate at the Maximum Power Point (MPP) for different illuminance levels. Therefore, a power/voltage management circuit is typically necessary to optimize the power conversion. A low-power switching regulator and its control

Table III. Typical Environment Illuminance Level and Commercial Available Solar Panel Energy Conversion Efficiency

		Indoor Light	Outdoor Light
Illuminance level (lux)		100–1000 lux	1000–65,000 lux
Solar Panel Energy Conversion Efficiency	c-Si	3–8%	∼18%
	a-Si	2–5%	8–13%
	GaAs	2∼8%	7–15%

scheme are required to track the maximum power point (MPPT). Other power management circuits, such as a quick charge circuit, may also be important to optimize other aspects of system operation such as minimization of start-up time.

Many aspects of system design will be application dependant such as form factor, cost, and operational duty cycle of the WSN. However, this article focuses on the system effectiveness and efficiency of the energy harvester. Thus, the goals for design of an efficient system should include the following:

—correct analysis of the energy available through measurement of the indoor light energy characteristics;
—selection of a high-efficiency PV cell for indoor light;
—design system operation voltage close to the Maximum Power Point (MPP);
—use of an energy storage that can efficiently store the energy and deliver it to the load.

In the following sections, these design goals are used as guidelines and emphasized through the system design and components selections.

5. INDOOR LIGHT ENERGY SCAVENGING

In this section, the indoor light characterization, and selection of the appropriate photovoltaic cells components are discussed. The objective is to identify the most efficient photovoltaic cells for sub-mW indoor light illuminance.

5.1 Indoor Light Energy

Several features distinguish indoor light energy harvesting from the higher-power outdoor solar energy harvesting. Firstly, indoor light energy has limited overall illuminance compared to outdoor light energy. Indoor illuminance level generally ranges from 100 lux to 1000 lux, or 1∼2 orders of magnitude lower than the outdoor illuminance. Since the conversion efficiency of the PV cells also decrease with decreasing light irradiance, this results in an even lower converted energy Goetzberger et al. [2003].

Research on indoor light energy shows that for the illuminance level between 100 lux to 1000 lux in the indoor environment, the efficiency achieved by commercial available PV cells is typically between 2–8%. This efficiency is approximately 1/3 of the outdoor solar panel's conversion efficiency. Typical illuminance levels and conversion efficiencies are shown in Table III for several common solar cell types: crystalline Silicon (c-Si), amorphous Silicon (a-Si), and GaAs [Jäger-Waldau 2004; Glunz et al. 2002].

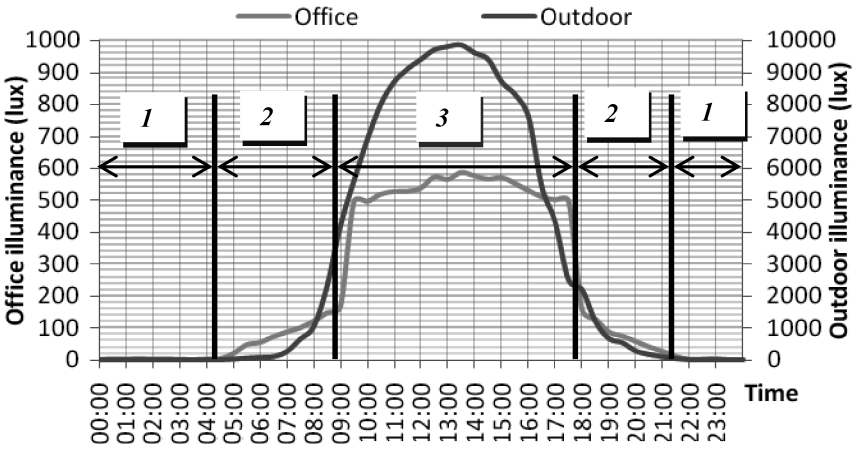

Fig. 4. Office and outdoor illuminance levels.

Secondly, for many indoor light energy harvesting scenarios, the major determinant of the illumination level is the level of artificial light. Since most of the artificial lights have fixed irradiance, the presence of these fixed irradiance artificial light sources leads to a relatively stable illuminance level on the PV cells. However, a typical room with windows will still have some contribution from a natural external light source. The effect of fixed artificial irradiance and variable natural irradiance is shown in Figure 4. These measurements were carried out in an office environment in late May, Ireland. In this case the room had one north-facing window and the light meter was placed 1.5 meters away from the window and directly under a 22 W ceiling fluorescent light (1.8 meters vertical distance). The illuminance results shown are the average data sampled over 72 hours.

As shown in Figure 4, the variability of the indoor light illuminance is largely due to the presence or absence of artificial light. Based on the illuminance level, a 24 hour period can be subdivided into three time periods, where each period lasts for approximately 8 hours. In period 1, due to lower than 10 lux illuminance, the harvestable light energy is negligible. Thus, the proposed energy harvesting device only focuses on harvesting light energy in period 2 and period 3. In these time periods, the target illuminance levels are 50 to 150 lux and 500 to 600 lux, respectively. The choice of PV cells should focus on these two illuminance levels, especially the latter, since over 85% of the available energy lies in this illuminance level.

Thirdly, it is the case that the different spectra of different indoor light sources can generate different responses on the photovoltaic cells. The same illuminance level, when generated from different light sources, can therefore result in different levels of power generation. Among the most common light sources, sunlight and halogen lights have a higher Power Spectral Density (PSD) on red light (near 656 nm) and fluorescent light and LED light has relatively high power density on the blue light wavelength (near 550 nm). The different materials and technologies used in solar cells will lead to different

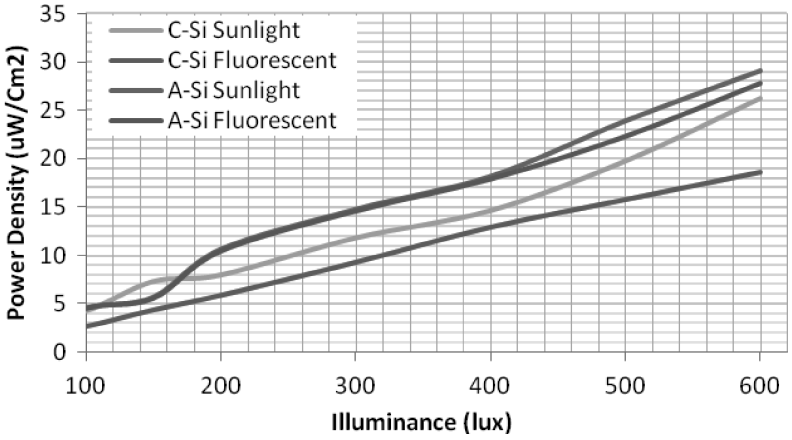

Fig. 5. Power spectral densities of light sources at various illuminance.

spectral responses and power densities. Figure 5 illustrates the differences of the power densities measured on crystalline silicon (SOLEMS 09/030/012) and amorphous silicon (Schott ASI2Oi05/055) solar panels when different light sources are used to generate the same illuminance level.

The crystalline silicon PV cell has a comparable power density when the light source is sunlight or halogen lights. However, the power density on this crystalline silicon PV cell declines 30.7% when the light source changes to fluorescent light. The same level of variation on power density was not found for amorphous Silicon PV cell, thus indicating that the amorphous silicon-based cells are more suitable for indoor applications.

5.2 Photovoltaic Characteristics

Based on the considerations outlined earlier, a solar panel with higher conversion efficiency in indoor environments and high sensitivity to the typical indoor fluorescent light spectrum is selected.

The Schott Solar's ASI2Oi05/055 utilizes an amorphous Silicon deposition on a glass substrate and the cell is based on a-Si PIN technology [Meier et al. 2004]. The active area of a module is 50 mm x 13.5 mm. The solar panel's measured I-V characteristics and P-V characteristics are shown in Figure 6. The maximum power under 100 lux, 200 lux, and 500 lux are 12.7 μW, 39.0 μW, and 151.6 μW, respectively. The average power generated from one PV cell over 24 hours, with an illuminance profile similar to that shown in Figure 4 was found to be 55.3 μW.

These PV and IV characteristics show the solar panel has a similar behavior to a voltage limited current source. The open circuit voltage is significantly less affected by different illuminance levels compared to the short-circuit current. The voltage limited current source-like IV characteristics show two features of the solar panel. Firstly, for any set illuminance level the current output is relatively constant over a wide voltage range, therefore the Maximum Power Point (MPP) is most likely to occur at high voltage level-operation. Secondly,

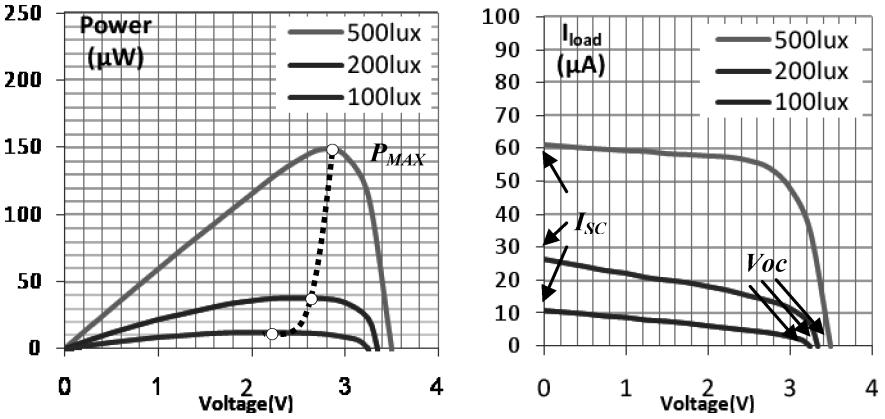

Fig. 6. The P-V and I-V characteristics of the Schott Solar's. ASI2Oi05/055/014JF.

for lower illuminance levels (100 lux and 200 lux), there is a relatively wide voltage range for which the power is close to the Maximum Power Point (MPP).

6. MAXIMUM POWER POINT TRACKING (MPPT) ISSUES

To enable the solar panel to operate at close to maximum power point in any illuminance level, a Maximum Power Point Tracking (MPPT) scheme is often used to change the voltage and current on the photovoltaic cells. The most commonly used approach for outdoor solar panel MPPT is perturb-and-observe. This method requires a microcontroller or DSP to continuously monitor the solar panel output and continuously control a switching regulator, by means of a hill climbing algorithm, to ensure maximum power output. The switching regulator controls the output voltage of the solar panel, and delivers the energy to the load. The perturb-and-observe method can accurately track the MPP, and the response time over abrupt changes on input is also short. To implement the perturb-and-observe approach, two core components, a control-unit (microcontroller or DSP) and a switching regulator, are essential. However, the major drawback of this MPPT system is the relatively high power consumption of these components. The MPPT scheme could be implemented by using a dc-dc converter such as the TI buck/boost converter (TPS63012) , controlled by the Tyndall mote's ATmega128L microcontroller, and a 32 KHz low-power oscillator. However, using this scheme the MPPT tracker's power consumption is calculated to be approximately 20 mW, assuming the microcontroller operates on a 4 MHz frequency and consumes 16.5 mW of power, a dc-dc converter efficiency of 55% (when the output current is approximately 100 μA) and a power consumption of 40 μW. The power consumption is thus much higher than the average power required over one sense and transmit cycle (116 μW for the 1 minute cycle). In the 500 lux illuminance condition, for each Schott Solar cell, the maximum power output is measured at 151.6 μW. Clearly this type of MPPT scheme is not feasible for low-power indoor applications.

A simpler and less energy costly MPPT method is the fractional open circuit voltage approach [Alippi and Galperti 2006]. Instead of using a microcontroller

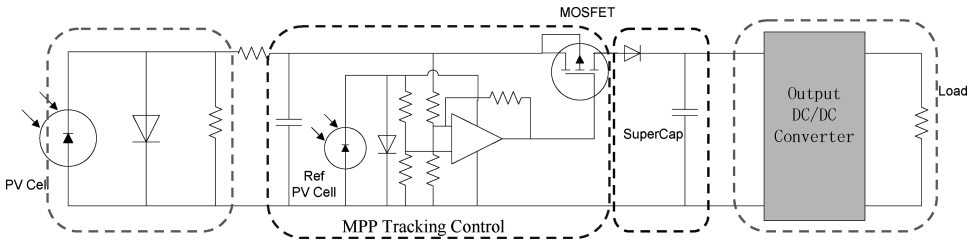

Fig. 7. Simplified FVOC MPPT circuit design.

or DSP to continuously control the switching regulator, this method uses an analog voltage comparator and regulates the solar cell voltage to be a fixed fraction of its open circuit voltage. This approach is based on the fact that the maximum power point operation voltage V_{mpp} and the open circuit voltage V_{oc} have a near linear correlation K_{fvoc}. The relation between these two can be described by Eq. (3).

$$V_{mpp} \approx V_{fvoc} = V_{oc} \cdot K_{fvoc} \tag{3}$$

A simplified circuit of a fractional open circuit voltage MPP tracker is shown in Figure 7.

This MPP tracker consists of two main parts, namely, the MPP tracking control unit and main MOSFET switch (includes a current limiting circuit). In the tracking control unit, a reference voltage is required to set V_{fvoc}. A secondary PV cell is used to obtain this reference voltage. By using the same photovoltaic technology as the main PV cell, the reference PV cell has the same open circuit voltage V_{oc}. A pair of resistors is then used to divide the open circuit voltage V_{oc} to the required V_{fvoc}.

A hysteresis voltage comparator is used as a control unit. It generates control signals to drive the MOSFET switch by comparing the reference V_{fvoc} and the main PV cell operational voltage. By adjusting the hysteresis, the threshold voltage of the comparator and the oscillation can be changed, thus, the sensitivity of the MPP tracking can be adjusted. The controlled MOSFET can then approach the theoretical maximum power point voltage $K_{fvoc} * V_{oc}$ by oscillating around the required voltage range.

To maximize the accuracy of the MPPT, it is necessary to find the optimum value of the K_{fvoc} factor. Some researchers consider the factor K_{fvoc} as a set of constants ranging from 0.71 to 0.78, depending on the photovoltaic panel's material characteristics and illuminance conditions [Raghunathan et al. 2005]. Other research asserts that the K_{fvoc} could simply be considered as a constant value of 0.74, to give a $+/-5\%$ error in maximum power point voltage evaluation [Alippi and Galperti 2008]. However, for the lower illuminance level encountered in indoor applications and for the Schott amorphous silicon, the value of the constant K_{fvoc} differs from the previous values discussed in the literature. For the Schott solar cell under 500 lux, 200 lux, and 100 lux fluorescent light conditions, K_{fvoc} can be seen to be 0.81, 0.80, and 0.76, respectively. A simulation was conducted to find the optimal single value of K_{fvoc} to enable the MPP tracker operate on highest efficiency considering the variation in illuminance

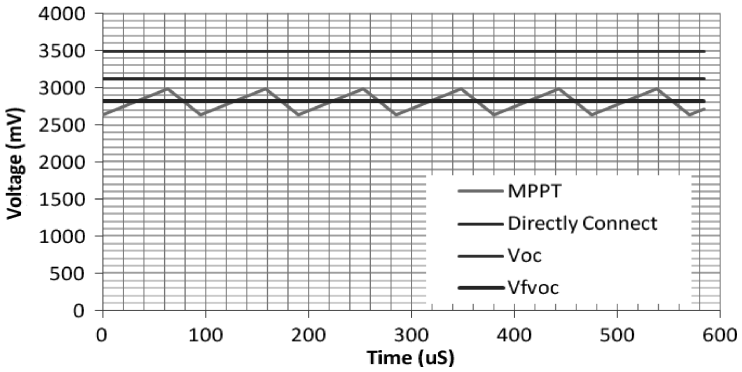

Fig. 8. MPPT simulation result at 500 lux illuminance.

levels shown in Figure 4. As indicated in Figure 4, under the same light sources, the different illuminance levels provide different percentages of overall light power generated by the PV cells. Eq. (4) is used to describe the average power generated across the entire 24 hour period. We have

$$P_{PV} = \sum_{k=0}^{n} P_{luxk} * \alpha_k = \sum_{k=0}^{n} V_{fvoc} * I * \alpha_k, \tag{4}$$

where P_{luxk} is the power generated when the operational voltage is the fixed fractional operation voltage V_{fvoc} under k lux illuminance, and α_k is the percentage of the total time period when this illuminance level persists. By measuring the time period, we consider the generated power to consist of 550 lux, 200 lux, and 100 lux for a time percentage α_k of 33%, 10%, and 11%, respectively. Tests were carried out to determine the power-voltage characteristics when various loads are applied on the PV cell under these different illuminance levels and the operating voltage corresponding to maximum power was determined for each case. The results show that the highest average P_{pv} was obtained when the fractional correlation K_{fvoc} is 0.806.

The proposed MPP tracker was then simulated using a PSPICE model by using the concept shown in Figure 7. Ultra low-power components are used to minimize the power consumption of the MPP tracker. The voltage comparator is a Seiko Instruments S-89530A, which consumes a typical 3 μW power. The analog switch used in the circuit is an Intersil ISL43L120 switch having power consumption less than 10 μW. Including the simulated power consumption of the other discrete components, the average power consumption of this maximum power point tracker is estimated at 28 μW. The simulation result (illuminance = 500 lux, $V_{oc} = 3.5$ V) is shown in Figure 8.

As indicated in Figure 8, when directly connecting the PV cells and the load, the voltage on the PV cells output is approximately 3.2 V so that the operation power point drifts away from the maximum power point. When the fractional MPP tracking method is used, the operational voltage of the PV cells oscillates around the proposed maximum power point voltage V_{fvoc}, which is proportional to the open circuit voltage V_{oc}, with a constant of proportionality of K_{fvoc}.

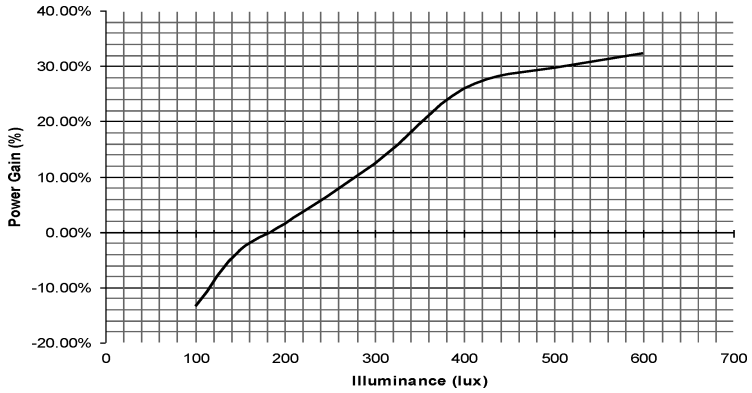

Fig. 9. Power gain from MPPT.

The results show the voltage on the PV cell output has an average of 2.8 V, with a positive error at +6.1% and a negative error at −6.7%. The equivalent internal resistance of the MPP tracker and the PV cells is 10 Ω. The close approximation to the theoretical MPP voltage and the relatively small power consumption of the MPP tracker give the PV cells output a significant power gain. The power gain can be calculated by comparing the power obtained if no MPPT is used to the power obtained with the f_{voc} MPPT. This power gain can be described by Eq. (5). We have

$$Gain = \frac{n(P_{MPP} - P_{Dir}) - P_L}{n * P_{Dir}}, \tag{5}$$

where n is the number of PV cells used in the light energy harvester, P_{MPP} is the average power generated from the PV cells with the MPP tracker, P_{Dir} is the average PV cell's power when it is directly connected with the load without MPP tracking, and P_L is the power consumed by the MPP tracker. The power loss will not increase linearly with the number of PV cells, as the controller power is fixed and the efficiency of the converter increases at larger output power. Therefore higher gain can be obtained from the MPP tracker by increasing the number of PV cells.

When the PV cells are directly connected to the load, the average power P_{Dir} generated from one PV cell over 24 hours with an illuminance profile similar to that shown in Figure 4 was found to be 41.3 μW. In the same deployment environment, when using the MPPT method, the average power P_{MPP} from each Schott PV cell is 53.5 μW. Hence, for each PV cell, the power gained from the MPPT $P_{MPP} - P_{Dir}$ is 12.2 μW. The average power consumption of the MPP tracker P_L is approximately 28 μW based on the simulation and the available component's characteristics. Therefore, to meet the power consumption requirement of the mote (116 μW) shown in Section 3 and the power consumption of the MPP tracker, at least 3 PV cells are required in this module. Considering the supercapacitor leakage current and other power consumption in the system, a PV cell bank with 4 Schott cells is utilized in the final prototype module described later.

Figure 9 shows the percentage of the power gained for particular illuminance levels calculated by Eq. (5). It can be seen from this graph that for 4 Schott cells and 200 lux illuminance level, the power gained by implementing the MPPT circuit is approximately offset by the power consumed by the MPPT circuit. However, for illuminance levels above 200 lux there is an overall gain in power. Therefore, in the target office scenario, by using the ultra low-power maximum power point tracking method, a 30% power gain can be obtained when the illuminance level is 500 lux. Over an entire 24 hour period the average power gain is calculated to be only 12.4%, because for light levels less that 200 lux there is a net consumption of power by the MPPT circuit.

7. ENERGY STORAGE ELEMENTS

As discussed in the previous section, the voltage limited current source behavior of the solar panel requires an energy storage element to separate the electric load and the PV panel. By placing an energy storage element between the PV panel and the load, the PV panel-based power supply will have a voltage source-like behavior, similar to a battery, and hence a more stable voltage output.

Three types of energy storage elements are frequently used in energy harvesting systems, namely, Nickel Metal Hydride rechargeable batteries, Lithium ion rechargeable batteries, and electrochemical double-layer capacitors (also known as supercapacitors or ultracapacitors). There are several significant differences between the characteristics of these storage elements. Supercapacitors have a lower energy density (energy/weight) than NiMH and Li-ion rechargeable batteries, typically 20Wh/kg compared to 70Wh/kg and 160Wh/kg, respectively [Tarascon and Armand 2001]. However, supercapacitors have higher power density (energy/time) than the rechargeable battery. The higher power density allows the supercapacitor to be charged more quickly than the rechargeable battery. The supercapacitors also have a much higher number of charge-discharge cycles than any current battery technology. Normally, it has over one million full charge-discharge cycles (deep cycles) compared to a rechargeable battery which has less than 1000 cycles [Conway et al. 1998]. Thus, for supercapacitors, replacement is unlikely to be required over its operational lifetime. The charging circuit for a rechargeable battery is more complicated than those required for supercapacitors. This increase in system complexity is more significant in solar panel-based harvesters, since the solar panel's intrinsic voltage limited current source characteristics make it difficult to charge the battery with a constant current. In addition, the Li-ion battery also requires a deep-discharge protection circuit, further increasing the system complexity. On the negative side, however, supercapacitors typically have a larger leakage current than rechargeable batteries and therefore the high self-discharge rate can be a major constraint for the supercapacitors' long-term energy storage capability.

When choosing a supercapacitor for this application, the ESR (Equivalent Series Resistance) of the capacitor can be an important factor. In Section 3, the power consumption pattern of the mote shows that a relatively large current

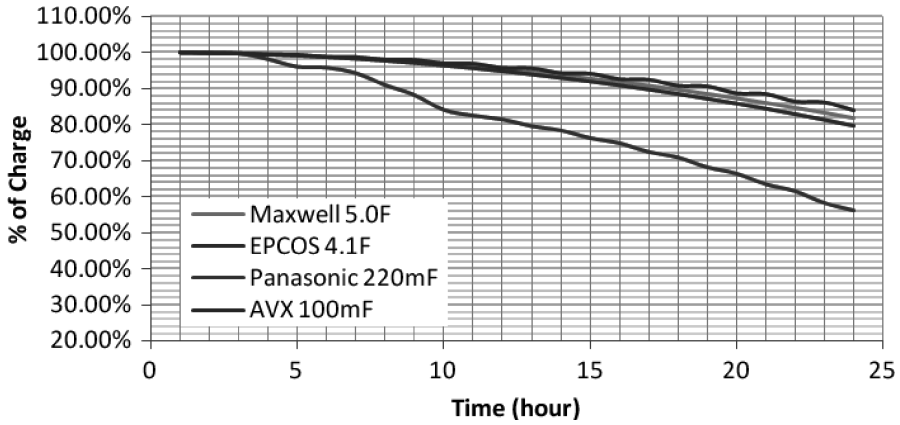

Fig. 10. Supercapacitor self-discharge rate test.

is drawn during the active mode. When this current is drawn from a supercapacitor with a high ESR it will result in a large voltage drop on the capacitor. The microcontroller's threshold voltage is 2.5 V, therefore if the voltage drop across the ESR is larger than 0.8 V (3.3 V–2.5 V), the microcontroller will be disabled, and the data processing and transmission will fail. For example, the small form factor Panasonic SD series EECS0HD104 has a 75 Ω ESR, and the active mode current is 33.1 mA, which will result in a voltage drop as high as 2.1 V. To avoid this, it is essential to use low ESR supercapacitors (e.g., AVX Bestcap supercapacitors, which have an ESR of 50 mΩ) to supply at least the active mode current. So one solution is to use a parallel connection of small, high energy density, but large ESR supercapacitors with lower energy density, lower ESR supercapacitors. For example, when the AVX supercapacitors are parallel connected with the Panasonic SD supercapacitor, the voltage drop during active mode can be kept less than 0.9 mV.

Another very important consideration for the use of the supercapacitor is the leakage current. However, useful data on the leakage is not always readily available in the supercapacitor datasheets. For this work, the leakage characteristics of individual supercapacitors have been measured to identify this important parameter in various types of supercapacitors.

To determine the leakage current over every 24 hours, tests were conducted on 4 different supercapactiors. All the supercapacitors were precharged to the same voltage level. They were then isolated and the voltage drop was monitored. The voltage drop is assumed to only be due to the self-discharge of the supercapacitors. The test result is shown in Figure 10.

These results confirm that the Self-Discharge Rates (SDR) of the supercapacitors are considerably higher than those of rechargeable batteries (5–10% monthly self discharge rate). The supercapacitors have SDR range from 45% to 15% every 24 hours. Therefore, without an intermittently available energy source every few days, using the supercapacitors alone as a long-term storage solution is infeasible. The average self-discharge current over the 24 hours is calculated and shown in Table IV.

Table IV. Leakge Current of Supercapacitors

Manufacturer	Capacitance Cs (F)	Average Leakage Current I_{leak} (uA)	Correlation ρ I_{leak}/Cs (uA/F)
Maxwell	5.00	27.78	5.56
EPCOS	4.10	26.28	6.41
Panasonic GoldCap	0.22	2.02	9.18
AVX Bestcap	0.10	0.52	5.2

As expected, there is a relationship between capacitance value and leakage current, although the values of leakage current per farad are similar. For a large supercapacitor (> 5 F), the leakage current is of the same order as of low duty cycle current consumption of the Tyndall mote. Clearly, therefore, the leakage characteristics of the supercapacitor can have a significant impact on the operation time of the mote in the absence of light. To more accurately scale the capacitance in order to determine the mote operation lifetime in the absence of light, Eq. (6) is then used. Here I_{mote} is the current consumption of mote, V_{full} is the voltage on the fully charged supercapacitor, V_{th} is the threshold operational voltage of mote, t is the required discharge time from V_{full} to V_{th}, (i.e., the required operation time in the dark), and ρ is the supercapacitor leakage current per farad.

$$C_S = \frac{I_{Mote} * t}{(V_{full} - V_{th}) - \rho * t} \tag{6}$$

Another important consideration for the supercapacitor is the time required for charging. It is commonly considered as relatively short compared to the rechargeable battery. For example, small supercapacitors can typically be charged to operational voltage within a couple of hours instead of over 10 hours in batteries. However, for the large supercapacitors, the charging time may be well beyond the charging time of the rechargeable batteries. Since the target operational scenario for the WSN requires a start-up stage every morning, a quick-charge circuit is therefore necessary to shorten the supercapacitor charging time.

One approach to quick charging is maximize the charging current of the PV cells by switching between parallel or series connection of the PV cells. This principal of the quick-charge circuit is similar to the proposed design introduced in Wolf and Enslin [1994]. However, the power consumption of the design reduced by almost 3 magnitudes, from 10mA to less than 20μA level. In order to obtain such change, the quick-charge circuits have been redesigned entirely.

As introduced in Wolf and Enslin [1994], the charging current is a variable depending on the number of PV cells, the PV cell charging voltage (V_{CH}), the voltage on the supercapacitor (V_{SC}), the energy harvester internal resistance (r), and supercapacitor Equivalent Series Resistance (ESR). The charging voltage after the MPP tracker circuit is considered as an ideal voltage source with an internal resistance. The simulation of the parallel and series connections of the PV cells are shown in a PSPICE model as illustrated in Figure 11.

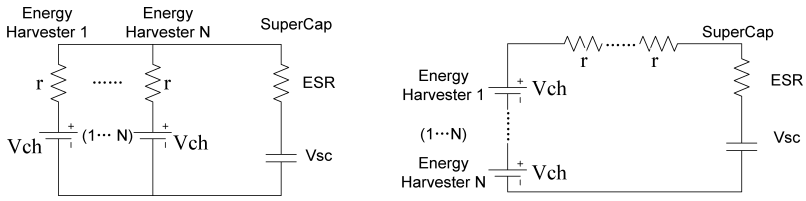

Fig. 11. Parallel and series connection configuration of PV cells.

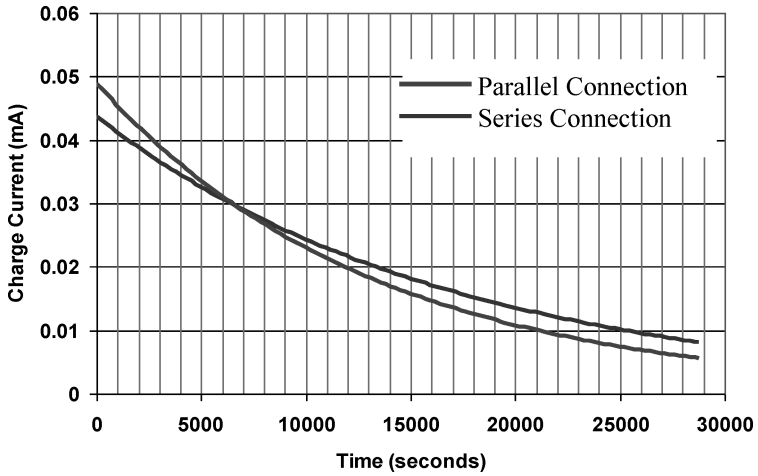

Fig. 12. Charging current of parallel and series configurations.

The charging currents in the preceding two configurations are derived in Eq. (7) and Eq. (8).

$$I_{parallel} = \frac{N * (V_{CH} - V_{SC})}{r + ESR} \tag{7}$$

$$I_{Series} = \frac{N * V_{CH} - V_{SC}}{N * r + ESR} \tag{8}$$

The simulation shows that at the initial stage of the charge, the charging current will be higher when the PV cells are connected in parallel. In a later stage, the charging current is higher for the series connection configuration. Figure 12 shows the simulation result of the charge current when the two types of connections are used.

The threshold voltage for the change between parallel and series connection is when $I_{parallel} = I_{Series}$. Using Eq. (7) and Eq. (8), the change from parallel connection to series connection occurs at the voltage level given in Eq. (9).

$$V_{SW} = \frac{N * r}{(N+1) * r + ESR} * V_{CH} \tag{9}$$

As introduced in the previous paragraph, the ESR of the supercapacitor is approximately 50 mΩ, whereas the internal resistance of the PV cell and the

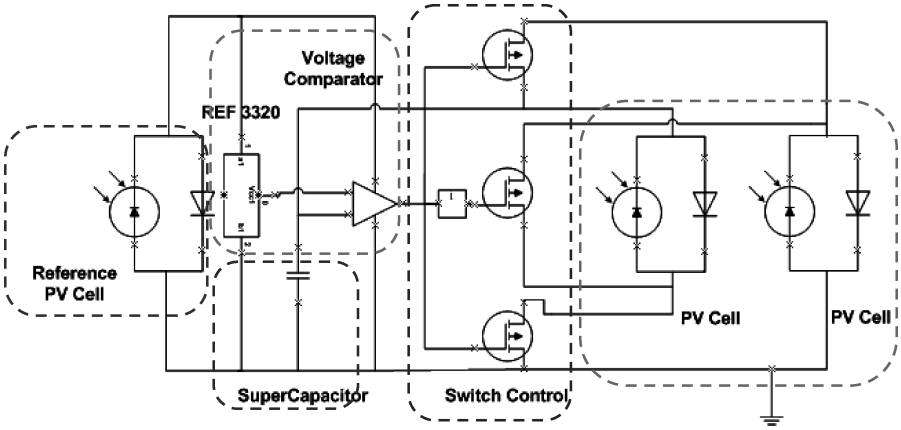

Fig. 13. Simplified quick-charge circuit.

MPP tracker is 10 Ω. Thus, the dominant resistance which determines the voltage at which to switch is the internal resistance of the energy harvester instead of the supercapacitor.

In order to achieve the switch in the connection from parallel to series, a voltage comparator with a logic output is used to control the switching. The supercapacitor voltage V_{SC} is monitored by the voltage comparator, and the required switch threshold voltage V_{SW} is compared with V_{SC}. Once $Vsc \geqq V_{SW}$, the logic inverter will then switch off the parallel connection and change to series connection. Vice versa, if $Vsc < V_{SW}$, the series connection switches back to parallel connection. Figure 13 shows the simplified design of the quick-charge circuit.

The same voltage comparator (Seiko Instruments S-89530A) is used in the circuit as the one used earlier in the MPP tracker. To set the reference voltage V_{SW}, the reference PV cell and an ultra low-power voltage reference IC (Texas Instruments REF3322) is used. Together with the low-power switches (Intersil ISL43L120) the average power consumption of the quick-charge circuit is calculated to be 25.7 μW. The simulation result for a 4 solar cell quick-charge circuit is shown in Figure 14. In this simulation, the supercapacitors are charged from 1.66 V. This initial voltage is the voltage which will remain on the capacitors after 8 hours in the absence of light and assuming a capacitor self-discharge rate comparable to those measured in Figure 7. The result was compared with the supercapacitor charge time when a parallel connection configuration is used.

The simulation result shows that after the switch from parallel to series connection at V_{SW} (2.2 V), the significantly higher charging current accelerates the charge. 95% of the final voltage V_{CH} is reached after 10030 seconds (2.78 hours) by using a parallel-only connection; the same value is obtained after 5050 seconds (1.4 hours) by using the quick-charge configuration. Thus the charging time is shortened by 1.38 hours or 50% of the parallel connection charging time.

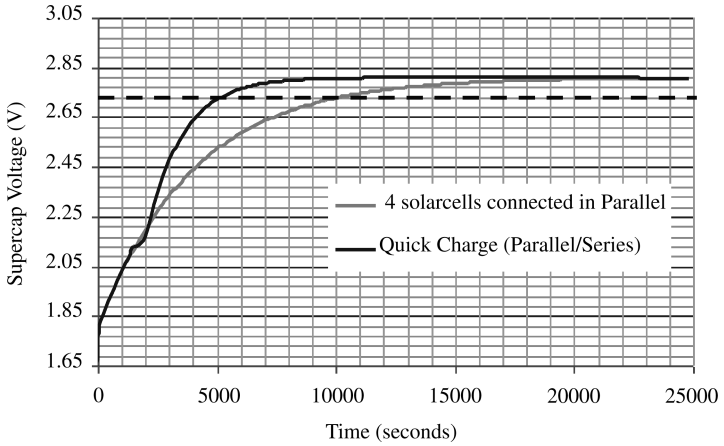

Fig. 14. Charge time comparison in two connection configurations.

8. SYSTEM IMPLEMENTATION AND EVALUATION

To validate the previous design considerations, a PV cell powered wireless sensor module prototype has been implemented by using commercial off-the-shelf components. The components were carefully selected in order to maximize the energy harvesting and minimize the power consumption within the prototype. Four 50mm $*$ 13.5mm Schott ASI2Oi05/055 amorphous silicon PV cells are used as the main power supply. One additional Schott cell (30mm $*$ 10mm) is used as the reference PV cell to provide the MPPT reference voltage V_{fvoc}. The voltage comparator is a Seiko Instruments S-89530A, which features a nano Ampere current consumption. A low ESR energy storage unit is included to avoid sudden voltage drop in the active mode of the mote. The selected energy storage unit is an EDL 2.3 V 10 F supercapacitor. The supercapacitor features a low leakage capacitance correlation ρ (I_{leak}/Cs) at 4.32. An additional DC/DC converter (TI TPS61200) is used to step up the supercapacitor voltage to 3V where required by Tyndall mote. The Tyndall mote is programmed to operate with a Sensirion SHT71 temperature and relative humidity sensor at a 0.1% duty cycle. A photodiode is connected to Tyndall mote in order to record the daily illuminance. Figure 15 shows the indoor light energy harvesting prototype.

In a target deployment scenario, an average 500 lux illuminance is available for 12 hours from 8:00AM to 8:00PM as shown in Figure 4. To emulate such an environment in the evaluation experiment, a common 22 W overhead fluorescent lamp is used as the light source. The distance between the prototype and the light source is 1.8 meters. The prototype is then adjusted to a position/angle that it extracts an average 500 lux illuminance. A data acquisition system (ADC-11-10) from Pico Technology is used to record the experiment.

Figure 16 shows the experimental results of the MPPT circuits. The PV cell's output voltage (connected to a 30 uF buffer capacitor) follows the maximum power voltage V_{mpp} with an asymmetric triangle wave. The proposed prototype can effectively track the MPP voltage within its $-$ 5% to $+$ 7% range. The K_{fvoc}

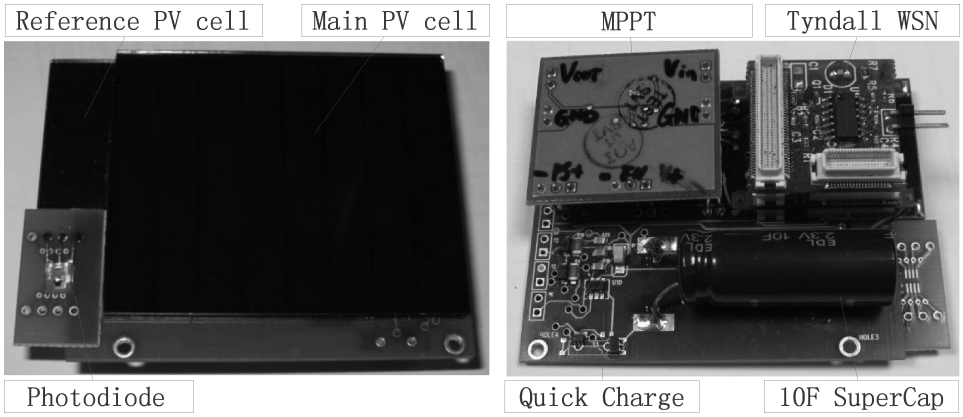

Fig. 15. PV-panel based energy harvester.

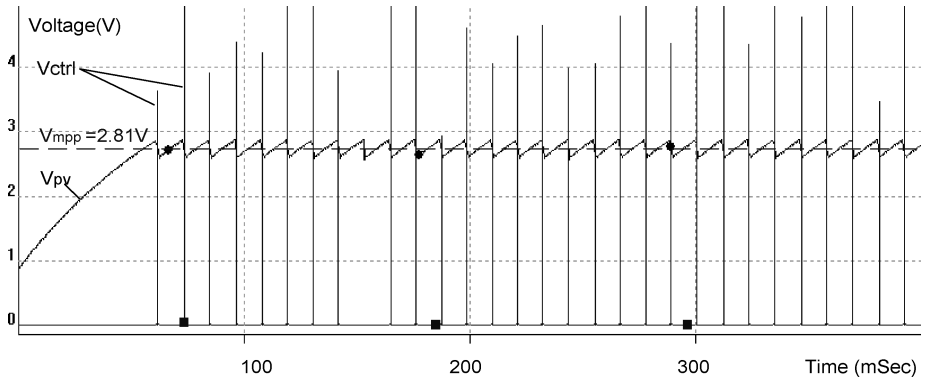

Fig. 16. MPPT experimental results.

obtained in the MPPT circuits is 0.76. Compared to the ideal fraction K_{fvoc} at 0.81, the result is within the +/− 8% range of the ideal maximum power point.

The power gain from using the proposed MPPT circuits is shown in Figure 17. A previously built non-MPPT PV cell energy harvesting prototype is used to compare and evaluate the present version. The prototype with the MPPT function shows an excellent result on the power gain. The employment of the MPPT circuits achieves a 27% power increase when 500 lux illuminance is applied. Multiple experiments were also conducted to investigate the efficiency of the MPPT method in other light levels. As shown in Figure 17, the proposed MPPT method increases the PV cell power output once the illuminance is higher than 250 lux. The current consumption of the MPPT circuit (ground pin current) is less than 15 μA. This result outperforms previous designs significantly and enables the MPPT methodology to be employed in sub-mW PV cell powered system.

A voltage monitoring circuit is also implemented in order to read the voltage level of the supercapacitor. Two switches are also incorporated, one to activate

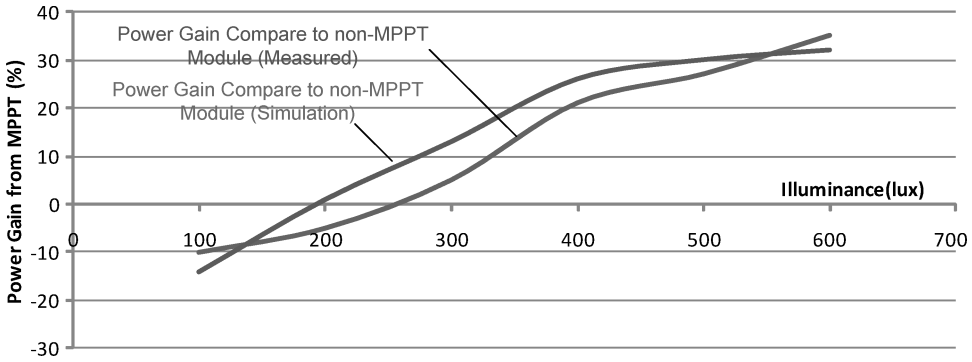

Fig. 17. Power gain from MPPT.

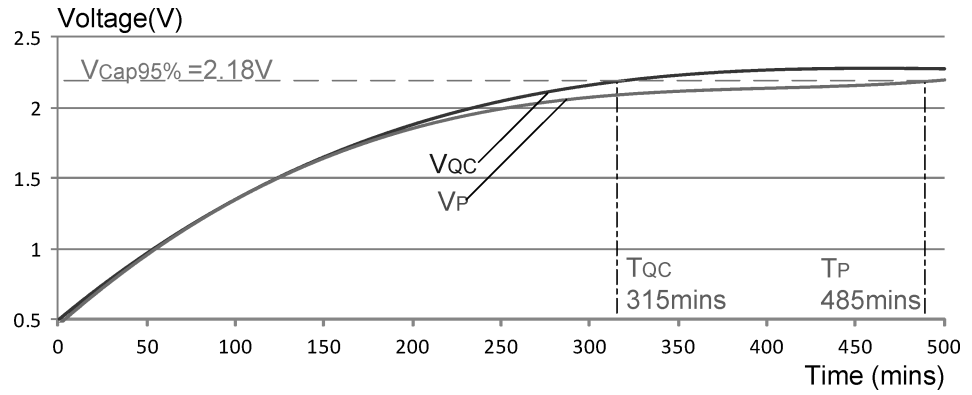

Fig. 18. Quick-charge circuits testing results evaluation.

the voltage monitoring function and connect it to Tyndall mote's microcontroller, the other to manually switch on or off the MPPT circuits in the module (when switched off, the PV cells directly connect to the supercapacitor). By using the voltage monitoring circuits and the MPPT switch, the MPPT function is deactivated; in this way, a test was conducted to investigate the effectiveness of the quick-charge circuits individually. The experimental results are illustrated in Figure 18, where V_P is the supercapacitor voltage when the PV cells are parallel connected, and V_{QC} is the capacitor voltage when the quick-charge circuit is employed.

Both supercapacitors were precharged to 25% of the supercapacitor voltage rating, and then the two configurations were charged in an identical environment. The result appears that the $V_{Cap95\%}$ (95% of the supercapacitor voltage rating) is obtained in 315 minutes (5.25 hours) by implementing the quick-charge circuit; the same value is achieved after 485 minutes (8 hours) by using the parallel connection configuration. The charging time was shortened by 34% when the quick-charge circuits were used.

The operational performance of the PV energy harvester module was then investigated by several experiments. For the first test the supercapacitor was precharged from a power supply to 1.5 V. The module was then connected with

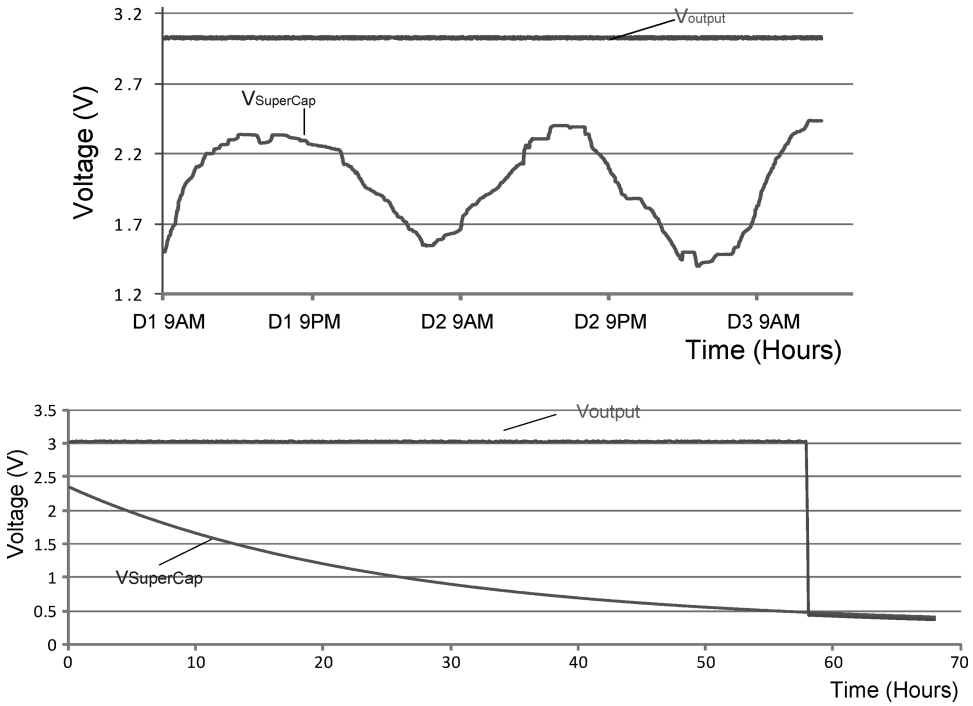

Fig. 19. (a) Performance evulation of energy harvester (office environment); (b) performance evulation of energy harvester (darkness).

the Tyndall mote in the target office environment (500 lux illuminance 8AM to 8PM, <30 lux 8PM to 8AM as illustrated in Figure 4), and tested over a 48 hour period. Figure 19(a) plots the supercapacitor voltage between Day-1 9am to Day-3 7pm. The lowest voltage point is 1.48 V, 3 times higher than the lower threshold voltage of the DC/DC converter (500 mV). The mote was able to correctly measure and transmit data for the entire period and the voltage on the Tyndall mote stabilized at 3.02 V.

Figure 19(b) plots the voltage on the supercapacitor in the absence of light, that is, where the power consumption of the mote is derived exclusively from the supercapacitor. Normal operation of the mote lasted for 58 hours, while the voltage of the capacitor gradually dropped to the DC/DC converter's threshold voltage. At this point the mote automatically enters deep-sleep mode and waits for power restoration.

These measured results show the indoor light powered wireless sensor module can operate autonomously during the presence of a typical indoor light illuminance. But it is unable to continuously operate in a total absence of light illuminance over a longer period of time. The MPPT method introduced in this article increases the PV cell's output power by 30% in a typical office lighting environment. The current consumption of the MPPT subsystem is less than 15 μA. The ultra low-power consumption is one order of magnitude lower than the previously known MPPT methods [Brunelli et al. 2009]. The negative side

of this MPPT circuit is that in this configuration, the supercapacitor can only be charged when the PV cell voltage is higher than the capacitor voltage. This negative impact is partly offset by the chosen amorphous silicon PV cell characteristics, since these PV cells can obtain a relatively high voltage in low illuminance. It is also offset by the low voltage ($<$2.3V) on supercapacitors, because the voltage on the PV cells are higher than 2.5 V once illuminance is higher than 300 lux, allowing the PV cells always operate above the supercapacitor voltage. The quick charge circuits provide a simple and effective way to accelerate the charging time of the supercapacitor by 34%. By implementing the design methods discussed in this article, the prototype enables small form factor PV cells to power a wireless sensor module with a stable output in a low-illuminance indoor condition. By eliminating the battery energy storage in the design, the prototype may greatly extend the system lifetime from present less than 6 months to 10$\sim$20 years.

9. CONCLUSION

This article presents and evaluates the environmental factors, component choice, design concepts, and main trade-offs in a PV panel-based energy harvesting WSN system design. The available light energy in the target deployment site has been carefully studied and the illuminance level and spectral power density in the target deployment area has been determined. Based on this, the PV cell bests suited for the indoor light energy harvesting has been chosen. The energy gains from using sub-mW maximum power point tracking have been evaluated. It can be concluded that with an ultra low-power design of the maximum power point tracker, the MPPT can improve the power conversion efficiency. However, a considerable percentage of power loss is attributed to the MPP tracker. For low-illuminance light energy harvesting, the power loss offsets most of the power gained from MPPT. The ultra-low current consumption of the MPPT subsystem enables the prototype increase the power harvested from the PV cells by 30% in a 500 lux lighting condition. The carefully simulated and successfully implemented design consumes less than 50 μW power, which is one magnitude lower than other known results. Quick charge circuits to shorten the system charging time have also been investigated. By using the parallel/series connections of PV cells, the start-up time of the mote is reduced by 34%. However, similar to the MPP tracking, the power loss on the quick-charge circuit is also a considerable part of the overall power consumption. A practical energy harvester module was designed and tested with a Tyndall 25mm mote system, and the performance has been presented and evaluated. Autonomous operation, during the presence of a typical real-life indoor light illuminance, indicates the feasibility of indoor light energy harvesting for wireless sensor network applications.

Interesting further research exists in several areas, one of which is to prolong the operation time in a dark environment by optimizing the energy storage elements, and also the possible implementation of an ultra low-power maximum power point tracker to increase the energy conversion efficiency of the MPPT.

REFERENCES

ALIPPI, C. AND GALPERTI, C. 2008. An adaptive system for optimal solar energy harvesting in wireless sensor network nodes. *IEEE Trans. Circ. Syst. I 55*, 6, 1742–1750.

BARTON, J., O'FLYNN, B., BELLIS, S., LYNCH, A., MORRIS, M., AND O'MATHUNA, S. C. 2005. A miniaturised modular platform for wireless sensor networks. In *Proceedings of the European Conference on Circuit Theory and Design*. 3, 35–38.

BRUNELLI, D., MOSER, C., THIELE, L., AND BENINI, L. 2009. Design of a solar-harvesting circuit for batteryless embedded systems. *IEEE Trans. Circ. Syst. I 56*, 11, 2519–2528.

CHULSUNG, P. AND CHOU, P. H. 2006. AmbiMax: Autonomous energy harvesting platform for multi-supply wireless sensor nodes. In *Proceedings of the 3rd Annual IEEE Communications Society Conference on Sensor and Ad Hoc Communications and Networks*. 1, 168–177.

CONWAY, B. E., BIRSS, V., AND WOJTOWICZ, J. 1998. The role and utilization of pseudocapacitance for energy storage by supercapacitors. *J. Power Sources*, 1-2, 1–14.

DOMS, I., MERKEN, P., MERTENS, R., AND VAN HOOF, C. 2009. Integrated capacitive power-management circuit for thermal harvesters with output power 10 to 1000uW. In *Proceedings of the IEEE International Conference on Solid-State Circuits*. 300–301.

DOYLE, M., FULLER, T. F., AND NEWMAN, J. 1993. Modeling of galvonostatic charge and discharge of the lithium/polymer/insertion cell. *J. Electrochem. Soc. 6*, 1526–1533.

ENERGY CONSERVATION MANAGEMENT, INC. 2006. Green and competitive—The energy, environmental, and economic benefits of fiber glass and mineral wool insulation products. http://www.naima.org/pages/resources/library/html.

GLUNZ, S. W., DICKER, J., ESTERLE, M., HERMLE, M., ISENBERG, J. ET AL. 2002. High-Efficiency silicon solar cells for low-illumination applications. In *Proceedings of the 29th IEEE Photovoltaic Specialists Conference*. 450–453.

GOETZBERGER, A., HEBLING, C. AND SCHOCK, H. W. 2003. Photovoltaic materials, history, status and outlook. *Mater. Sci. Engin.: R: Rep. 40*, 1, 1–46.

GRIGG, P. AND SLATER, A. 2004. Assessment of energy efficiency impact of building regulations compliance report. Building Research Establishment. http://www.eeph.org.uk/uploads/documents/partnership/.

HARTE, S., O'FLYNN, B., MARTINEZ-CATALA, R. V., AND POPOVICI, E. M. 2007. Design and implementation of a miniaturised, low power wireless sensor node. In *Proceedings of the 18th European Conference on Circuit Theory and Design*. 894–897.

HAYES, M., WANG, W. S., O'DONNELL, T., O'FLYNN, B., AND O'MATHUNA, S. C. 2009. Energy harvesting for practical deployment of wireless sensor networks in building energy management (BEM) applications. In *Proceedings of the NanoPower Forum*. 102–105.

HERMLE, M., DICKER, J., WARTA, W., GLUNZ, S. W. AND WILLEKE, G. 2003. Analysis of edge recombination for high-efficiency solar cells at low illumination densities. In *Proceedings of the 3rd World Conference on Photovoltaic Energy Conversion*. 1009–1012.

JÄGER-WALDAU, A. 2004. Status of thin film solar cells in research, production and the market. *J. Solar Energy 77*, 6, 667–678.

JIANG, X., POLASTRE, J., AND CULLER, D. 2005. Perpetual environmentally powered sensor networks. In *Proceedings of the 4th International Symposium on Information Processing in Sensor Networks.* 463–468.

KING, A. W., DILLING, L., ZIMMERMAN, G. P., FAIRMAN, D. M., HOUGHTON, R. A. ET AL. 2007. North American carbon budget and implications for global carbon cycle. United States DoC Online Library. www.climatescience.gov/Library/sap/.

KRIKKE, J. 2005. Sunrise for energy harvesting products. *IEEE Pervas. Comput. 4*, 1, 4–5.

MEIER, J., SPITZNAGEL, J., KROLL, U., BUCHER, C., FAŸ, S., MORIARTY, T., AND SHAH, A. 2004. Potential of amorphous and microcrystalline silicon solar cells. *J. Thin Solid Films*, 451-452, 518–524.

MENZEL, K., PESCH, D., O'FLYNN, B., KEANE, M., AND O'MATHUNA, C. 2008. Towards a wireless sensor platform for energy efficient building operation. *J. Tsinghua Sci. Technol. 13*, S1, 381–386.

PEREYMA, M. 2007. Overview of the modern state of the vibration energy harvesting devices. In *Proceedings of the International Conference on Perspective Technologies and Methods in MEMS Design*. 107–112.

RAGHUNATHAN, V., KANSAL, A., HSU, J., FRIEDMAN, J., AND SRIVASTAVA, M. 2005. Design consideration for solar energy harvesting wireless embedded systems. In *Proceedings of the 4th International Symposium on Information Processing in Sensor Networks*. 457–462.

RAGHUNATHAN, V., GANERIWAL, S., AND SRIVASTAVA, M. 2006. Emerging techniques for long lived wireless sensor networks. *IEEE Comm. Mag. 44*, 4, 108–114.

RANDALL, J. F. 2005. *Designing Indoor Solar Products: Photovoltaic Technologies for AES.* John Wiley & Sons.

ROUNDY, S. WRIGHT, P. K., AND RABAEY, J. M. 2003. *Energy Scavenging for Wireless Sensor Networks: With Special Focus on Vibrations*. Kluwer Academic Publishers.

ROUNDY, S., LELAND, E. S., BAKER, J., CARLETON, E., REILLY, E. ET AL. 2005. Improving power output for vibration-based energy scavengers. *IEEE Pervas. Comput. 4*,1, 28–36.

SHENCK, N. S. AND PARADISO, J. A. 2001. Energy scavenging with shoe-mounted piezoelectrics. *IEEE Comput. Soc. J. Micro 21*, 3, 30–42.

SIMJEE, F. I. AND CHOU, P. H. 2008. Efficient charging of supercapacitors for extended lifetime of wireless sensor nodes. *IEEE Trans. Power Electron. 23*, 3, 1526–1536.

TARASCON, J. M. AND ARMAND, M. 2001. Issues and challenges facing rechargeable lithium batteries. *Nature 414*, 6861, 359–367.

WOLF, S. M. M. AND ENSLIN, J. H. R. 1993. Economical, PV maximum power point tracking regulator with simplistic controller. In *Proceedings of the Power Electronics Specialists Conference*. 581–587.

Received July 2009; revised February 2010; accepted February 2010